Electron Interactions With BCl_3

Cite as: Journal of Physical and Chemical Reference Data **31**, 971 (2002); https://doi.org/10.1063/1.1504440
Submitted: 27 December 2001 . Accepted: 01 July 2002 . Published Online: 31 October 2002

L. G. Christophorou, and J. K. Olthoff

Electron Interactions With BCl_3

L. G. Christophorou[a] and J. K. Olthoff[b]

Electricity Division, Electronics and Electrical Engineering Laboratory, National Institute of Standards and Technology, Gaithersburg, Maryland 20899-8113

(Received 27 December 2001; revised 17 June 2002; accepted 1 July 2002; published 31 October 2002)

In this paper we review and assess the cross sections for collisions of low-energy electrons with boron trichloride (BCl_3). The only available experimental cross section data are for partial and total ionization and electron attachment, and the electron attachment cross sections are uncertain. Calculated values are available for the total elastic, differential elastic, and momentum transfer cross sections, and derived cross sections have been published for vibrational excitation and dissociation. Other than some rather uncertain data on electron attachment rate constants and some measurements of electron drift velocities in BCl_3/Ar and BCl_3/He mixtures, there are no measurements of the electron attachment, ionization, or transport coefficients for this gas. Analysis of the experimental data on the electron affinity, electron attachment, and electron scattering, enabled identification of negative ion states of BCl_3 at about -0.3, 1.0, 2.8, 5.2, 7.6, and 9.0 eV. Because the existing electron collision data are few and uncertain, relevant data are provided for photon impact on BCl_3. [DOI: 10.1063/1.1504440]

Contents

List of Tables

[a]Electronic mail: lgchrist@otenet.gr
[b]Electronic mail: james.olthoff@nist.gov

List of Figures

1. Introduction

In earlier papers in this series we have pointed out the significance of electron collision data to models intended to aid in developing plasma processing techniques for the microelectronics industry. Modeling of such plasmas is often hindered by the absence of reliable electron-collision data. In our continuing effort to provide such data, we focus in this paper on boron trichloride (BCl_3).

The BCl_3 molecule is a major source of reactive radicals generated via electron-impact dissociative processes, including electron attachment. For this reason, it is widely used as a plasma processing gas in the etching of metals (e.g., aluminum) and semiconductors (e.g., GaAs and Si) (see, for example, Refs. 1–7). BCl_3 is used in a variety of gas mixtures (i.e., BCl_3 mixed with Ar, N_2, Cl_2, SF_6, CF_4, CHF_3, $Ar+O_2$, $Ar+Cl_2$, $Ar+CCl_2F_2$, $Ar+SF_6$, $Ar+H_2+N_2$, $SiCl_4+H_2$, and $Ar+Cl_2+N_2$) for the etching of GaAs, GaSb, GaN, GaP, InAs, InP, AlGaAs, AlGaP, AlGaN, AlInAs, AlInP, InGaAs, InGaP, InAlP, InAlN, NiMnSb, and InGaAsP (e.g., see Refs. 7–13).

In this paper we review, assess, synthesize, discuss, and suggest cross sections for collisions of low-energy electrons with the BCl_3 molecule. The high reactivity and corrosiveness of the BCl_3 gas make experimental measurements difficult and partially account for the meager electron collision cross section data that are available for this gas at this time and their large uncertainties. Besides some rather uncertain data on electron attachment rate constants for BCl_3 (see Sec. 5) and some measurements of the electron drift velocity in BCl_3/Ar and BCl_3/He mixtures,[14] there are no measurements of the electron attachment, ionization, or transport coefficients for this gas. Because the existing electron collision data are few and uncertain, we provide relevant data involving photon impact with the BCl_3 molecule. For calculated cross sections for some electron collision processes for the Cl and BCl_2 fragments see McKoy *et al.*[15]

The review procedure followed in this paper is similar to that in our earlier studies.[16–25] In Table 1 are listed the cross sections and rate coefficients discussed in this paper along with their symbols and units.

2. Structural and Electronic Properties

Boron trichloride (BCl_3) is a nonpolar, plane symmetric (D_{3h} symmetry) molecule.[26] Its ground state outer valence shell molecular orbital configuration[27,28] is: $(2a_1')^2(2e')^4(1a_2'')^2(3e')^4(1e'')^4(1a_2')^2X\,^1A_1'$. The outermost three ($1a_2'$, $1e''$, and $3e'$) occupied valence orbitals are nonbonding (Cl lone pair), the $1a_2''$ orbital is B–Cl π bonding, and the $2a_1'$ and $2e'$ are B–Cl σ bonding. These six orbitals have binding energies between 10 and 20 eV.[27]

The lowest unoccupied molecular orbital of the BCl_3 molecule is $2a_2''$(B $2p$–Cl $3p\pi^*$), and the next two higher-lying empty orbitals are $3a_1'$ and $4e'$ (B $2p$–Cl $3p\sigma^*$).[29,30] The presence of these unoccupied molecular orbitals helps explain the observed negative ion states of the BCl_3 molecule, and consequently the observed or calculated structure in the electron scattering and electron attachment cross sections. A detailed calculation by Baeck and Bartlett[29]—optimizing bond lengths and bond angles within D_{3h} symmetry for BCl_3 and C_{3v} symmetry for BCl_3^-—provided a number of structural and electronic parameters such as ionization energies, electronic vertical excitation energies, and vibrational frequencies for the BCl_3, BCl_3^-, BCl_3^+ species.[29]

TABLE 1. Definition of symbols

Symbol	Definition	Common scale and units
$\sigma_{pa,t}(\lambda)$	Total photoabsorption cross section	10^{-18} cm^2; 10^{-22} m^2
$\sigma_{sc,t}(\epsilon)$	Total electron scattering cross section	10^{-16} cm^2; 10^{-20} m^2
$\sigma_{e,t}(\epsilon)$	Total elastic electron scattering cross section	10^{-16} cm^2; 10^{-20} m^2
$\sigma_{e,partial}(\epsilon)$	Partial elastic electron scattering cross section	10^{-16} cm^2; 10^{-20} m^2
$\sigma_{e,diff}(\epsilon)$	Elastic differential electron scattering cross section	10^{-16} cm^2 sr^{-1}
$\sigma_m(\epsilon)$	Momentum transfer cross section (elastic)	10^{-16} cm^2; 10^{-20} m^2
$\sigma_{i,partial}(\epsilon)$	Partial ionization cross section	10^{-16} cm^2; 10^{-20} m^2
$\sigma_{i,t}(\epsilon)$	Total ionization cross section	10^{-16} cm^2; 10^{-20} m^2
$\sigma_{a,t}(\epsilon)$	Total electron attachment cross section	10^{-16} cm^2; 10^{-20} m^2
$k_{a,t}(E/N)$	Total electron attachment rate constant	10^{-9} cm^3 s^{-1}
$w(E/N)$	Electron drift velocity	10^6 cm s^{-1}

A number of experimental studies contribute to an understanding of the molecular and electronic structure of the BCl_3 molecule. These include electron-impact excitation and ionization,[31–33] negative-ion formation,[31–37] electron-impact dissociation into excited fragments,[38–40] photoelectron spectra,[28,41,42] photoionization and photodissociation,[43–49] and photoabsorption and fluorescence measurements in the ultraviolet/visible (UV/VIS) region.[44–52] Some of the photophysical studies incorporated mass analysis and fluorescence measurements and established the fragmentation patterns of BCl_3 at specific photon wavelengths (see Sec. 4.3).

2.1. Total Photoabsorption Cross Section, $\sigma_{pa,t}(\lambda)$

The vacuum UV absorption spectrum of BCl_3 (absorbance versus wave number) has been measured by Planckaert *et al.*[51] from 200 to 120 nm. It has two well defined but broad bands with maxima near 57 970 cm^{-1} (7.187 eV, 173 nm) and 73 400 cm^{-1} (9.100 eV, 136 nm). Planckaert *et al.* assigned the lowest frequency band to a valence–shell transition of the $\pi^* \leftarrow \pi$ type, and described the second band as a Rydberg transition to a $3s$ orbital or as a valence-shell transition of the $\sigma^* \leftarrow \sigma$ type. Another measurement of the relative photoabsorption cross section of BCl_3 was made by Maria *et al.*[50] who reported a broad low-energy absorption band in the 200–220 nm region. Subsequently, Suto *et al.*[44] measured the total photoabsorption cross section, $\sigma_{pa,t}(\lambda)$, of BCl_3 as a function of the photon wavelength λ in the 106–190 nm range (Fig. 1). Suto *et al.* estimated the uncertainty in their measurements to be about $\pm 15\%$. According to Suto *et al.*, the peak at 129 nm is likely to be due to the impurity HCl which could be produced by the reaction of BCl_3 with water adsorbed on the wall of their gas handling system. Another photoabsorption cross section measurement was made by Lee *et al.*[45] at shorter wavelengths (45–106 nm). These measurements have an uncertainty of $\pm 15\%$ and are also shown in Fig. 1.

Measurements of the photoabsorption cross section of BCl_3 at still higher energies (190–280 eV) have been made by Ishiguro *et al.*[53] using synchrotron light. Synchrotron light was similarly employed by Ueda *et al.*[27] for the measurement of Auger electron spectra. The latter have also been investigated by Cini *et al.*[54] using 2 keV electrons.

In Table 2 are listed vertical and adiabatic ionization energies for the BCl_3 molecule, along with corresponding suggested assignments.

2.2. Electron Affinity and Negative Ion States of BCl_3

As indicated earlier in this section, the three lowest unoccupied molecular orbitals of BCl_3 are $2a_2''$, $3a_1'$, and $4e'$. These unoccupied molecular orbitals help explain the observed negative ion states of the BCl_3 molecule and, consequently, the observed structure in the electron scattering and electron attachment cross sections. Table 3 lists values of the electron affinity and negative ion states of the BCl_3 molecule and the vertical detachment energy of BCl_3^-, as determined by various methods. The experimental data in Table 3 (see also Fig. 2) identify negative ion states of BCl_3 at about -0.3, 1.0, 2.8, 5.2, 7.6, and 9.0 eV. The -0.3 and 1.0 eV values are associated with the lowest empty orbital $2a_2''$, the 2.8 eV value with the $3a_1'$ empty orbital, and the 5.2 eV value with the $4e'$ empty orbital. The 7.6 and 9.0 eV values are associated with the positions of electron-excited Feshbach resonances in the 6.0–10 eV energy range.

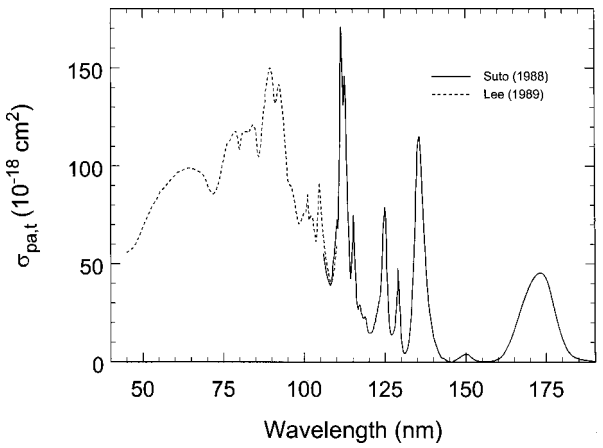

FIG. 1. Total photoabsorption cross section, $\sigma_{pa,t}(\lambda)$, for BCl_3: (——) Ref. 44; (- - -) Ref. 45.

TABLE 2. Vertical and adiabatic[a] ionization energies[b] of BCl_3

Ionization energy (eV)	Comment/ Orbital assignment	Reference	Method
10.9±0.2	Threshold energy[c,d] for the production of ground state BCl_3^+	55	EI–MS[e]
11.82 (11.60)	Values for the production of BCl_3^+	42	PES[f]
(11.60±0.01)	Adiabatic value for the production of BCl_3^+	43	PI–MS[g]
(11.16−11.44)[h]	Adiabatic values	29	C[i]
(11.48−11.74)[h]	Adiabatic values	29	C
11.49−11.83[h]	Vertical values	29	C
11.68−12.34[h]	Vertical values	29	C
11.60±0.02	Threshold energy for the production of BCl_3^+	43	PI–MS
11.64	Threshold energy for the production of $BCl_3^+(\tilde{X}\,^2A_2')+e$	45	PA[j]
11.67±0.15	Vertical value	56	EI[k]
11.72	Vertical value, $1a_2'^{-1}$	28	He I EPS[m]
11.73 (11.64)	$1a_2'$; $2a_2'^{n}$	41	PES
11.73 (11.64)	$\tilde{X}\,^2A_2'$	46	PA–SR[o]
11.78	$2a_2'$	58	C[p]
11.82 (11.60)	$\tilde{X}\,^2A_2'$	48,42	PES
11.97	e'	59	PES
12.03±0.02	"Appearance potential" for BCl_3^+	31	EI–MS
12.0±0.5	"Appearance potential" for BCl_3^+	60	EI–MS
12.19	Threshold energy for the production of $BCl_3^{+*}(\tilde{A}\,^2E'')+e$	45	PA
12.214 (ν=0)	$1e''^{-1}$	28	He I EPS
12.28	$2e''$	58	C[p]
12.30	Threshold energy for the production of $BCl_2^+ + Cl + e$	45	PA
12.30±0.02	Threshold energy for the production of $BCl_2^+ + Cl + e$	43	PI–MS
12.39 (12.19)	$1e''$; $2e''^{n}$	41	PES
12.39 (12.19)	$\tilde{A}\,^2E''$	46	PA–SR
12.43	a_2'	59	PES
12.65 (12.23)	$\tilde{A}\,^2E''$	48,42	PES
12.41	$7e'$	58	C[p]
12.608 (line 5)	$3e'^{-1}$	28	He I EPS
12.66	Threshold energy for the production of $BCl_3^+(\tilde{B}\,^2E')+e$	45	PA
12.66	$3e'$; $7e'^{n}$	41	PES
12.66	$\tilde{B}\,^2E'$	46	PA–SR
12.75	$\tilde{B}\,^2E'$	48,42	PES
12.77	e''	59	PES

2.3. Fundamental Vibrational Modes and Other Data

Herzberg[66] lists for the vibrational frequencies ν_1 (symmetric stretching), ν_2 (out-of-plane bending), ν_3 (asymmetric stretching), and ν_4 (asymmetric bending) of the BCl_3 molecule, respectively, the values of 471 cm^{-1} (0.0584 eV), 462 cm^{-1} (0.0573 eV), 958 cm^{-1} (0.1188 eV), and 243 cm^{-1} (0.030 eV). Stull and Prophet[67] list for ν_1, ν_2, ν_3, and ν_4, respectively, the values of 0.0584, 0.0583, 0.1223, and 0.0301 eV. Knowledge of these frequencies can be helpful in efforts to use infrared laser measurements of the extinction coefficient of this gas in a discharge to determine the rotational and translational temperature and degree of dissociation of the gas, as well as for plasma diagnostics (see, for example, Farrow[68]).

The vibrational frequencies of BCl_3^- are expected to lie energetically lower than the corresponding ones of the neutral molecule BCl_3. Jacox *et al.*[69] in a matrix isolation study of the interaction of excited Ne atoms with BCl_3 assigned an absorption band they observed at 686 cm^{-1} (0.085 eV) to the ν_3 of $^{11}BCl_3^-$, and Baeck and Bartlett[29] calculated values for all the vibrational frequencies of BCl_3^-. The averages of the two values they give for each frequency ν_1, ν_2, ν_3, and ν_4 of BCl_3^- in Table VII of their paper are, respectively, 551 cm^{-1} (0.068 eV), 320 cm^{-1} (0.0397 eV), 704 cm^{-1} (0.0873 eV), and 218 cm^{-1} (0.0270 eV).

In Table 4 are listed other data on BCl_3 and BCl_3^- which are relevant to the present discussion on the interactions of slow electrons with the BCl_3 molecule.

3. Electron Scattering

3.1. Total Electron Scattering Cross Section, $\sigma_{sc,t}(\epsilon)$

To our knowledge, there are no measured or calculated values of the total electron scattering cross section, $\sigma_{sc,t}(\epsilon)$, of BCl_3.

3.2. Total Elastic Electron Scattering Cross Section, $\sigma_{e,t}(\epsilon)$

There are no experimental measurements of the total elastic electron scattering cross section, $\sigma_{e,t}(\epsilon)$, of BCl_3. There are, however, a number of calculated values of the total (integral) elastic electron scattering cross section. Figure 3

TABLE 2. Vertical and adiabatic[a] ionization energies[b] of BCl_3—Continued

14.10	$2a_2''$	58	C[p]
14.22	Threshold energy for the production of $BCl_3^+*(\tilde{C}\ ^2A_2'')+e$	45	PA
14.240 ($\nu_1^+=0$)	$1a_2''^{l}$	28	He I EPS
14.40 (14.23)	$\tilde{C}\ ^2A_2''$	42	PES
14.41 (14.30)	$\tilde{C}\ ^2A_2''$	48	PES
14.42 (14.22)	$1a_2''$; $2a_2''^{n}$	41	PES
14.42 (14.22)	$\tilde{C}\ ^2A_2''$	46	PA–SR
14.50	a_2''	59	PES
15.27	$6e'$	58	C[p]
15.32	Threshold energy for the production of $BCl_3^+*(\tilde{D}\ ^2E')+e$	45	PA
15.320 (progression 6, $\nu=0$)	$2e'^{l}$	28	He I EPS
15.51 (15.28)	$\tilde{D}\ ^2E''$	42,48	PES
15.54 (15.32)	$2e'$; $6e'^{n}$	41	PES
15.54 (15.32)	$\tilde{D}\ ^2E''$	46	PA–SR
15.75	e'	59	PES
17.74 (17.74)	Threshold energy for the production of $BCl_3^+*(\tilde{E}\ ^2A_1')+e$	45,46	PA, PA–SR
17.74	$6a_1'$	58	C[p]
17.699 ($\nu_1^+=0$)	$2a_1'^{l}$	28	He I EPS
17.70 (17.70)	$\tilde{E}\ ^2A_1'$	48,42	PES
−(17.74)	$2a_1'$; $6a_1'^{n}$	41	PES
17.79	a_1'	59	PES
18.37	Threshold energy for the production of $BCl^+ + 2Cl + e$	45,43	PA, PI–MS

[a]Data in parenthesis are values designated by the corresponding authors as adiabatic.
[b]See Table 6 in Sec. 5 for electron impact values.
[c]Koski *et al.*[55] measured the thresholds 11.0±0.2, 10.9±0.2, 10.9±0.2, and 10.6±0.2 eV, respectively, for the production of $B^{10}Cl_2^{37}Cl^{35+}$, $B^{10}Cl_2^{35}Cl^{37+}$, $B^{11}Cl_3^{35+}$, and $B^{10}Cl_3^{35+}$.
[d]Koski *et al.*[55] measured mass spectrometrically the ionization threshold energies for the production of BCl_2^+ and BCl^+ by electron impact on BCl_3 and found them to be 7.20 and ~10.44 eV, respectively. Dibeler and Walker[43] estimated an ionization threshold for BCl_2=7.74 eV from photoionization studies.
[e]EI–MS=electron impact–mass spectrometry.
[f]PES=photoelectron spectroscopy.
[g]PI–MS=photoionization-mass spectrometry.
[h]The range of values corresponds to the results of various types of calculation.
[i]C=calculation.
[j]PA=photoabsorption.
[k]EI=electron impact.
[l]Probable orbital.
[m]He I EPS=He I excited photoelectron spectrum.
[n]Assignments of Berger *et al.*[57] based on their *ab initio* calculations.
[o]PA–SR=photoabsorption-synchrotron radiation.
[p]*Ab initio* calculation.

shows $\sigma_{e,t}(\epsilon)$ as calculated by a number of groups: Tossell *et al.*[30] using the multiple scattering $X\alpha$ method; Winstead and McKoy[15,78] using the Schwinger multichannel variational method in the static exchange approximation with and without inclusion of polarization; Isaacs *et al.*[62] using the complex Kohn method; and Bettega[63] using the Schwinger multichannel method with pseudopotentials at the static exchange polarization approximation. The inset in Fig. 3 shows an expanded view of the calculation of Isaacs *et al.* at low energies.

The contributions of the lowest unoccupied electronic states of BCl_3 to the magnitude and structure of $\sigma_{e,t}(\epsilon)$ shown in Fig. 3 can be seen from the calculated partial elastic electron scattering cross sections, $\sigma_{e,partial}(\epsilon)$, shown in Fig. 4. Figure 4(a) shows the $\sigma_{e,partial}(\epsilon)$ calculated by Tossell *et al.*[30] using the multiple scattering $X\alpha$ method. These results show the symmetry of the resonances which give rise to the peaks in the total elastic electron scattering cross section (see also Table 3). Figure 4(b) shows the polarized self-consistent field (SCF) results of Isaacs *et al.*[62] for the A_1, A_2, B_1, and B_2 symmetries. The A_1 cross section is very large as the electron energy approaches zero and shows two broad maxima at 2.5 and 5.5 eV. Although the polarized-SCF B_2 cross section does not show a distinct peak due to the negative ion (shape) resonance near 2 eV, it does show this feature in the static exchange calculation results. Figure 4(c) shows the $\sigma_{e,partial}(\epsilon)$ results of Bettega[63] to 50 eV.

3.3. Differential Elastic Electron Scattering Cross Section, $\sigma_{e,diff}(\epsilon)$

Figure 5 shows the differential elastic electron scattering cross section, $\sigma_{e,diff}(\epsilon)$, of BCl_3 calculated by Isaacs *et al.*[62] and Bettega[63] at several electron energies. Unfortunately, the

TABLE 3. Electron affinity and negative ion states of BCl_3 and vertical detachment energy of BCl_3^-

Value/Energy position (eV)	Method of determination	Comment/Assignment	Reference
Electron affinity			
0.33±0.2	Measurement[a]	Adiabatic	35
0.27 to 0.42[b]	Calculation	Adiabatic	29
>0.0	Swarm measurements	Formation of BCl_3^-	61
>0.0	Beam measurements	Formation of BCl_3^-	36,37
Negative ion states			
~0.9	Dissociative attachment producing Cl^-		37
1.1±0.1	Dissociative attachment producing Cl^-		32
<1.0	Electron transmission experiment/Calculation	a_2''	36,30
0.25[c]	Calculation	B_2	62
0.41–0.79[b]	Calculation	Vertical attachment energy	63
0.00–1.30	Calculation		64
~1.8	Calculation[d]	B_2	63
~2.6	Threshold-electron excitation[e]		32
2.86	Electron transmission experiment/Calculation	a_1'	36,30
2.5	Calculation[f]	A_1	62
5.16	Electron transmission experiment/Calculation	e'	36,30
5.5	Calculation[f]	A_1; B_1	62
~6.5	Dissociative attachment producing Cl^-		37
~7.6	Threshold-electron excitation[e]		32
~7.6	Electron transmission experiment/Calculation	Core-excited shape resonance[g]	36,30
~7.8	Dissociative attachment producing Cl^-		37
8.7	SF_6^- scavenger technique		32
9.05	Electron transmission experiment/Calculation	Core-excited shape resonance[g]	30,36
9.7	Threshold-electron excitation[e]		32
8.5	Calculation[d]	A_1, B_1	62
Vertical detachment energy			
1.77	Optogalvanic experiments		65
1.73–1.99[b]	Calculation		29

[a]Determined using collisions of Cs atoms with BCl_3.
[b]The range of values corresponds to the results of various types of calculation.
[c]The position of this B_2 symmetry shape resonance moves from ~2.0 eV in the static exchange calculation to 0.25 eV with the inclusion of polarization effects (see Isaacs *et al.*[62]).
[d]Static exchange approximation calculation.
[e]SF_6^- scavenger technique.
[f]Polarized-SCF calculations.
[g]Observed in electron transmission and in dissociative electron attachment experiments.

results of these two calculations can be compared at only one common energy (5.0 eV). There are no experimental measurements of $\sigma_{e,diff}(\epsilon)$ for this molecule.

3.4. Momentum Transfer (Elastic) Cross Section, $\sigma_m(\epsilon)$

Figure 6 shows the elastic momentum transfer cross section, $\sigma_m(\epsilon)$, of BCl_3 as calculated by McKoy and associates,[15,78] Isaacs *et al.*,[62] and Bettega.[63] The inset in Fig. 6 is an expansion of the results of Isaacs *et al.*[62] showing the B_2 resonance.

3.5. Inelastic Electron Scattering Cross Sections, $\sigma_{in}(\epsilon)$

3.5.1. Vibrational Excitation Cross Sections

Nagpal and Garscadden[72] derived three vibrational excitation cross sections for BCl_3 in the energy range 0–30 eV using the conventional ''two-term'' solution of the time-dependent Boltzmann transport equation and the electron drift velocity data for BCl_3/Ar and BCl_3/He mixtures of Mosteller *et al.*[14] These are shown in Fig. 7. The cross sections designated by $\sigma_{\nu 2,\nu 1}$, $\sigma_{\nu 4}$, and $\sigma_{\nu 3}$ are for the vibrational frequencies indicated by the subscripts. McKoy *et al.*[78] questioned these data on the basis that they are based on experimental measurements taken under conditions for which electron attachment is significant and this was not considered in the analysis.

3.5.2. Electronic Excitation Cross Sections

Cross sections for some electronic transitions of BCl_3 (and also of the BCl and BCl_2 fragments) have been computed by McKoy *et al.*[15]

3.5.3. Cross Sections for Dissociation into Neutral Fragments

Using the same experimental data and computational procedure as for the vibrational excitation cross sections (Fig. 7), Nagpal and Garscadden[72] derived two dissociation cross sections for BCl_3. These are shown in Fig. 7 and are designated by σ_{d1} and σ_{d2}. They refer, respectively, to the disso-

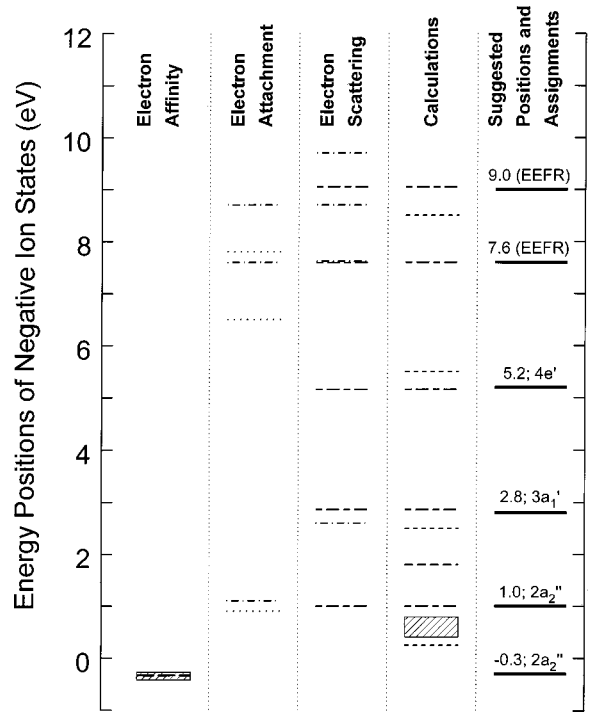

FIG. 2. Negative ion states of the BCl_3 molecule as determined by electron affinity measurements, electron attachment measurements, electron scattering measurements, and calculations: Electron affinity: (— — —) experimental data from Ref. 35, (////) calculations from Ref. 29; Dissociative electron attachment producing Cl^-: experimental data from (···) Ref. 37 and (—·—·—·—) Ref. 32; Electron scattering: experimental data from (—·—·) Refs. 36, 30 and (—·—·—·—) Ref. 32; Electron scattering: calculated results from (- - -) Ref. 62, (////) Ref. 29, (— — —) Ref. 63, and (—·—·) Ref. 30. The last column gives the suggested positions and assignments. It should be noted that the adiabatic position of the ~1.0 eV negative ion state is at about −0.3 eV [−|EA(BCl_3)|]. EEFR labels refer to assignments made from electron excited Feshbach resonance data.

TABLE 4. Other basic properties of BCl_3 and BCl_3^-

Parameter	Value	Reference
BCl_3		
Equilibrium distance R_{B-Cl}	1.754 Å, 1.755 Å	29
	1.754 Å	62
	1.751 Å[a]	70
	1.75 Å	67
	1.745 Å[b]	71
	1.742 Å	63
	1.742 Å	30
Dissociation energy		
BCl_2-Cl	4.78±0.02 eV	43
	~4.59 eV	61
	4.61 eV	72
$BCl+Cl_2$	5.65 eV	72
BCl–Cl	3.39±0.02 eV	43
B–Cl	5.51±0.04 eV	43
Polarizability	9.6×10^{-24} cm^3	12
	9.47×10^{-24} cm^3	73
	9.38×10^{-24} cm^3	73
	8.99×10^{-24} cm^3[c]	74
	8.21×10^{-24} cm^3[d]	75
Bond angle		
Cl–B–Cl	120°	67
BCl_3^-		
R(B–Cl)	1.876 Å, 1.879 Å[e]	29
	1.836 Å[f]	76
Bond angle[g]		
	107.3°, 107.6°[e]	29
	110.9°[f]	76

[a]Experimental value.
[b]CNDO/2 calculation.
[c]In plane electrical polarizabilty measured in dioxan.
[d]Mean polarizability.
[e]*Ab initio* calculations.
[f]Determined from studies of the molecular structure of donor-acceptor complexes of trimethylamine and boron trichloride.
[g]The BCl_2 radical is bent with a ClBCl angle of ~122° (see Franzi *et al.*[77]).

ciation processes leading to BCl_2+Cl and $BCl+Cl_2$ (see values of the energy thresholds for these processes in Table 4). In Fig. 7 is also plotted an estimate of the electron-impact dissociation cross section as computed by McKoy *et al.*[15] This latter cross section is essentially the sum of the cross sections they computed for electronic states presumed to be dissociative. In this regard, the estimated cross section by McKoy *et al.* for dissociation of BCl_3 into neutrals should at best be a lower limit value.

The cross sections of Nagpal and Garscadden[72] are observed to have a lower magnitude and to lie at lower energies than the cross sections of McKoy *et al.*[15] This has been attributed[15] to the neglect of the effect of electron attachment in the calculation of Nagpal and Garscadden, and to the fact that the dissociation energies are larger than the threshold values used by Nagpal and Garscadden.

4. Electron Impact Ionization

4.1. Partial Ionization Cross Sections, $\sigma_{i,partial}(\epsilon)$

An early electron-impact ionization study of BCl_3 by Marriott and Craggs[31] showed that the most abundant positive ion is BCl_2^+, followed by BCl_3^+. Subsequently, in a mass spectrometric study of the photoionization of BCl_3, Diebeler and Walker[43] found that the relative abundances of the positive ions BCl_3^+, BCl_2^+, BCl^+, and B^+ at 584 Å (21.23 eV) are: 0.59, 1.0, 0.072, and ~0.001. A more recent study of the fragmentation of valence electronic states of BCl_3^+ using photoelectron spectroscopy by Biehl *et al.*[42] found that between 11 and 19 eV the BCl_2^+ ion is produced from the fragmentation of the excited states of BCl_3^+.

The most detailed study of electron-impact ionization of BCl_3 was conducted by Jiao *et al.*[33] using Fourier transform mass spectrometry. They observed the formation of the parent positive ion BCl_3^+ and the fragment positive ions BCl_2^+, BCl^+, and Cl^+. The positive-ion fragments BCl^+ and Cl^+ were found to react with neutral BCl_3 to generate BCl_2^+ with bimolecular rate constants respectively equal to $(5.3\pm0.5)\times10^{-10}$ cm^3 s^{-1} and $(6.2\pm0.5)\times10^{-10}$ cm^3 s^{-1}. The BCl_2^+ ion was found not to react with BCl_3. Jiao *et al.*[33] did not observe B^+ or Cl_2^+, thus confirming the suspicion of Marriott and Craggs[31] that the observation of these two positive ions in their experiment was an artifact of pyrolysis on the filament. Table 5 lists the threshold energies (''appearance

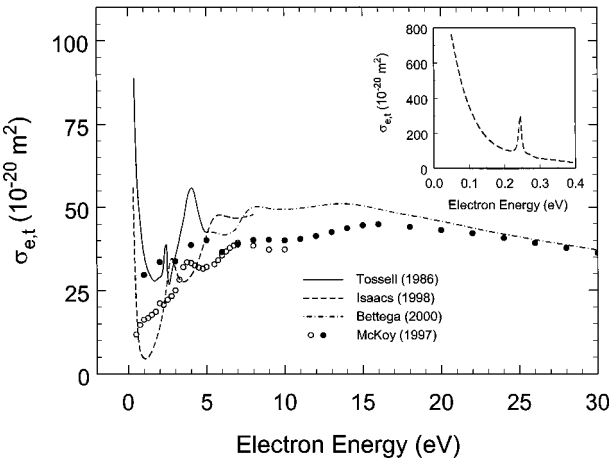

FIG. 3. Calculated total (integral) elastic electron scattering cross section, $\sigma_{e,t}(\epsilon)$, for BCl_3: (——) Ref. 30; (●) Ref. 15 static-exchange approximation without polarization; (○) Ref. 15 static-exchange approximation with polarization; (- - -) Ref. 62; (—·—·—·—) Ref. 63. (Inset) Low energy data of Isaacs *et al.*

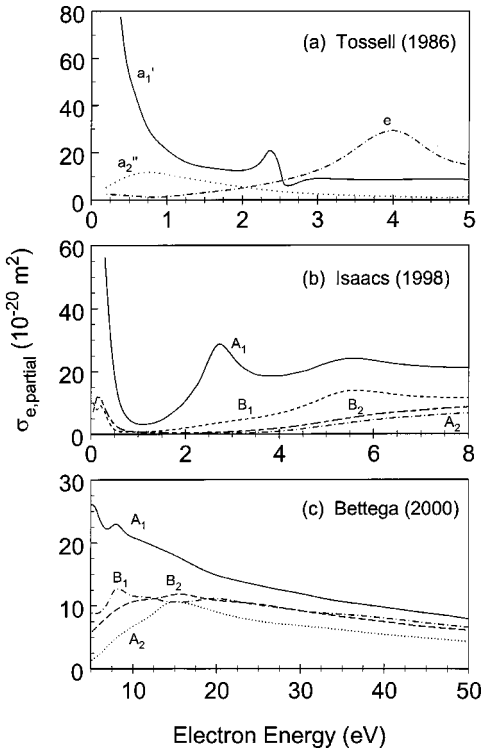

FIG. 4. Calculated partial elastic electron scattering cross sections, $\sigma_{e,partial}(\epsilon)$, for BCl_3 for the identified symmetries: (a) Ref. 30; (b) Ref. 62; (c) Ref. 63.

potentials'') of the various positive ions produced by electron impact on BCl_3.

Jiao *et al.*[33] measured the partial ionization cross sections, $\sigma_{i,partial}(\epsilon)$, of BCl_3 relative to the ionization cross section of argon and calibrated their data using the measurements of Wetzel *et al.*[80] and Krishnakumar and Srivastava[81] for Ar. They gave no uncertainty for the magnitude of $\sigma_{i,partial}(\epsilon)$, but the uncertainty in their energy scale was quoted as ± 0.5 eV. Their data for $\sigma_{i,partial}(\epsilon)$ are shown in Fig. 8 and are listed in Table 6. The cross section for BCl_3^+ is seen to be substantial. Interestingly, Overzet and Luo[82] in a study of ionization in rf plasmas of pure BCl_3 observed only the positive ions BCl_2^+, BCl^+, and B^+. The data of Jiao *et al.* show that from threshold to 60 eV the most abundant positive ion is BCl_2^+.

4.2. Total Ionization Cross Section, $\sigma_{i,t}(\epsilon)$

The sum of the partial ionization cross sections of Jiao *et al.*[33] for BCl_3^+, BCl_2^+, BCl^+, and Cl^+ has been plotted in Fig. 9 and is taken to represent the total ionization cross section, $\sigma_{i,t}(\epsilon)$, of BCl_3. Values of these data for electron energies $\leqslant 30$ eV are listed in Table 7. These data represent our suggested values, but they should be considered a lower limit to $\sigma_{i,t}(\epsilon)$. To our knowledge there are no other measurements of $\sigma_{i,t}(\epsilon)$. According to Becker[83] the preliminary measurements by Tarnovsky and Becker quoted in Deutsch *et al.*[84] need further scrutiny. In Fig. 9 the measurements of Jiao *et al.* are compared with the calculated values obtained using the modified additivity-rule (MAR),[84,85] the Deutsch–Märk (DM) formalism,[85] and the binary encounter-Bethe (BEB) theory.[86] Below 30 eV, the latter calculation gives $\sigma_{i,t}(\epsilon)$ values in better overall agreement with the experimental results of Jiao *et al.*, thus the results of this calculation may be also preferred above ~30 eV. However, significant discrepancies exist among the available data and the need for more investigation is evident.

4.3. Dissociation of BCl_3 by Electron and Photon Impact

Besides the calculated results discussed in Sec. 3.5.3, there are no measurements of the cross section for electron-impact dissociation of BCl_3 into neutral fragments. However, there have been a number of studies on electron-impact-induced dissociation[38–40,87] and photon-impact-induced dissociation[44–49] of BCl_3 and identification of the resultant (excited) radicals via their fluorescence emissions. The results of these electron-impact and photon-impact studies are briefly elaborated upon in this section, since they provide useful spectroscopic data for the identification of the species in plasma reactors containing BCl_3.

Jabbour *et al.*[38] measured the absolute photoemission cross section of the $BCl^* A\,^1\Pi \rightarrow X\,^1\Sigma^+$ system around 2720 Å produced by dissociative electron impact on BCl_3. This system is used for optical plasma diagnostics. The cross section was found to rise from the threshold at 14.0 ± 1.5 eV to a maximum near 25 eV and then to rise again to its overall maximum at near 40 eV. The maximum cross section value was measured to be 2.3×10^{-18} cm^2 with an uncertainty of $\pm 20\%$. In a subsequent study, Gilbert *et al.*[39] reported photoemission cross sections and appearance potentials for the most intense UV emissions produced by electron-impact dis-

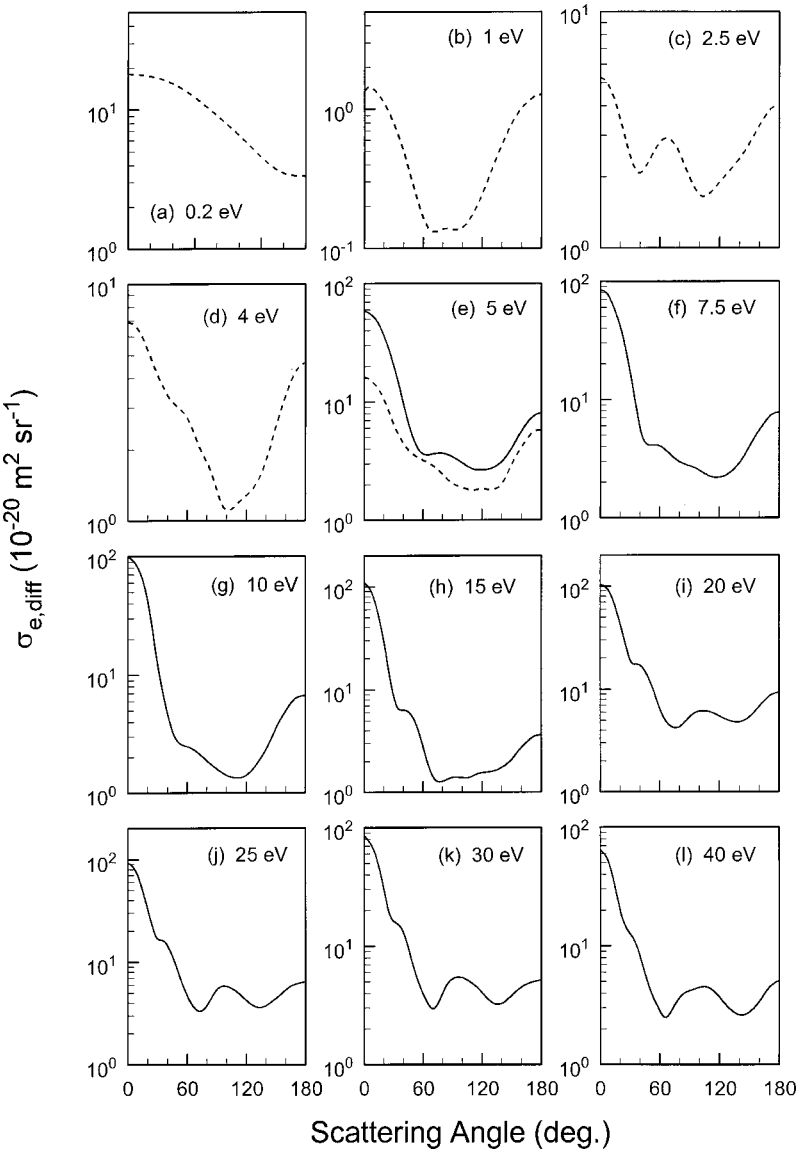

FIG. 5. Calculated differential elastic electron scattering cross sections, $\sigma_{e,diff}$, for BCl_3 for a number of electron energies: (- - -) results of Isaacs *et al.*;[62] (——) results of Bettega.[63]

sociation of BCl_3. In particular, Gilbert *et al.*[39] studied the two atomic boron emissions B* $2p^2\,{}^2D \rightarrow 2p\,{}^2P^0$ line at 208.9 nm and B* $3s\,{}^2S \rightarrow 2p\,{}^2P^0$ line at 249.8 nm, and the BCl* $A\,{}^1\Pi \rightarrow X\,{}^1\Sigma^+$ system around 272.4 nm. The 249.8 nm boron line was found to have the largest emission cross section (5.4×10^{-18} cm^2) at 75 eV. The BCl $A\,{}^1\Pi \rightarrow X\,{}^1\Sigma^+$ emission cross section around 272.4 nm was found to be 3×10^{-18} cm^2 at 40 eV, which is ~20% higher than their earlier measurement.[38] Figure 10 shows the emission spectrum recorded by Gilbert *et al.*[39] in the wavelength range 200–300 nm, generated by impact of 200 eV electrons on BCl_3. The two B* lines at 208.9 and 249.8 nm and the BCl* $A\,{}^1\Pi \rightarrow X\,{}^1\Sigma^+$ emission band around 272.4 nm are clearly seen in the figure. The radiative lifetime of the BCl* A state [for the spectrally unresolved (0,0), (1,1) and (2,2) bands at 272 nm] was measured by Hesser[87] to be 19.1 ns.

Figures 11(a) and 11(b) give, respectively, the emission cross sections measured by Gilbert *et al.*[39] for the BCl* $A\,{}^1\Pi \rightarrow X\,{}^1\Sigma^+$ band and the B* $3s\,{}^2S \rightarrow 2p\,{}^2P^0$ line at

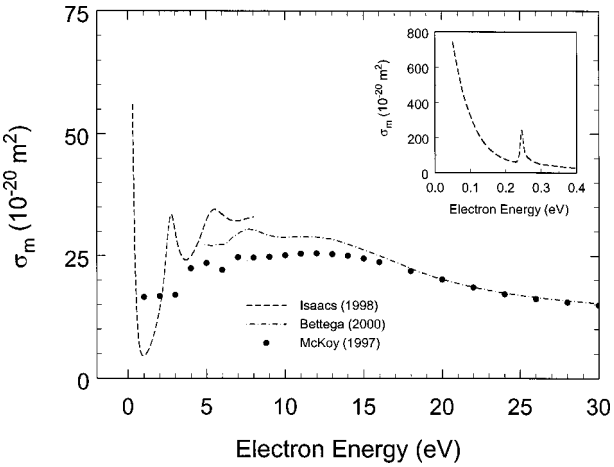

FIG. 6. Calculated elastic momentum transfer cross section, $\sigma_m(\epsilon)$, for BCl_3: (●) static-exchange approximation result from Ref. 15; (- - -) Ref. 62; (—·—·—·—) Ref. 63. (Inset) Expanded results by Isaacs *et al.* from Ref. 62 showing the B_2 resonance.

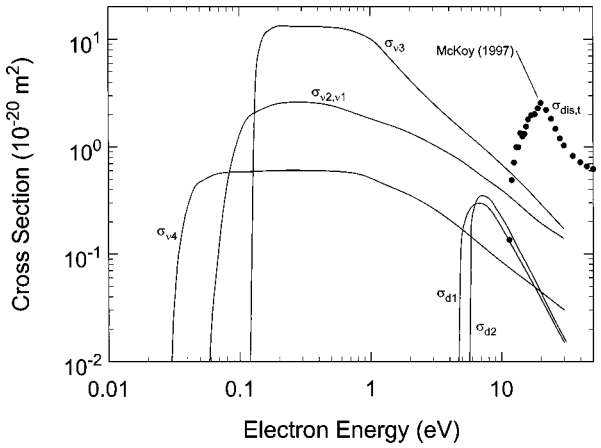

FIG. 7. Derived collisional cross sections for BCl_3 by Nagpal and Garscadden in Ref. 72: (——), cross sections $\sigma_{\nu 2,\nu 1}(\epsilon)$, $\sigma_{\nu 4}(\epsilon)$, and $\sigma_{\nu 3}(\epsilon)$ for the vibrational modes indicated by the subscripts, and cross sections $\sigma_{d1}(\epsilon)$ and $\sigma_{d2}(\epsilon)$ for the dissociation processes leading to BCl_2+Cl and $BCl+Cl_2$, respectively. (●) Computed cross section, $\sigma_{dis,t}(\epsilon)$, for dissociation of BCl_3 by electron impact from Refs. 15 and 62 (see text).

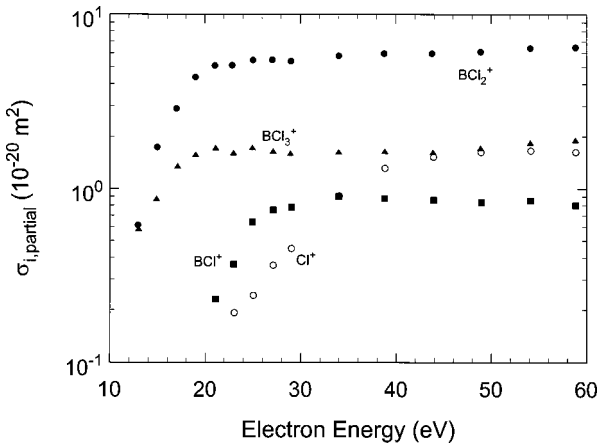

FIG. 8. Partial electron-impact ionization cross sections, $\sigma_{i,partial}(\epsilon)$, for BCl_3 from Jiao *et al.*[33]

249.8 nm as a function of the electron energy from threshold to 100 eV. Based on the data in Tables 8 and 9, the two onsets at 14.0 and 29.0 eV [indicated by the arrows in Fig. 11(a)], have been ascribed,[39] respectively, to the dissociation processes

$$BCl_3^* \rightarrow BCl^*(A\ ^1\Pi) + 2Cl \qquad (1)$$

and

$$BCl_3^* \rightarrow BCl^*(A\ ^1\Pi) + Cl + Cl^+. \qquad (2)$$

Similarly, on the basis of the data in Tables 8 and 9, the two onsets at 22.0 and 34.0 eV [indicated by the arrows in Fig. 11(b)] have been ascribed,[39] respectively, to the dissociation processes

$$BCl_3^* \rightarrow B^*(3s\ ^2S) + 3Cl \qquad (3)$$

and

$$BCl_3^* \rightarrow B^*(3s\ ^2S) + 2Cl + Cl^+. \qquad (4)$$

Tokue *et al.*[40] also investigated the emission spectra of excited fragments generated by electron impact on BCl_3 in the wavelength range 190–600 nm for electron energies up to 110 eV. Their cross section measurements for the $B^*\ 3s\ ^2S \rightarrow 2p\ ^2P^0$ transition and the $BCl^*\ A\ ^1\Pi \rightarrow X\ ^1\Sigma^+$ band are compared with the measurements of Gilbert *et al.*, respectively, in Figs. 11(a) and 11(b). The cross section values for these emissions—and also for the $B^*\ 2p^2\ ^2D \rightarrow 2p\ ^2P^0$ transition—are compared in Table 10 for 100 eV electrons. Although the cross section value of Gilbert *et al.* for the transition $B^*\ 2p^2\ ^2D \rightarrow 2p\ ^2P^0$ is about a factor of 2 lower than that of Tokue *et al.*, the agreement between the measurements of the two groups is generally good. In addi-

TABLE 5. Threshold energies[a] (''appearance potentials'') of positive ions produced by electron impact on BCl_3

Positive ion fragment	Threshold energy (eV)	Reference
$B^{10}Cl_2^{37}Cl^{35+}$	11.0±0.2	55
$B^{10}Cl_2^{35}Cl^{37+}$	10.9±0.2	55
$B^{11}Cl_3^{35+}$	10.9±0.2	55
$B^{10}Cl_3^{35+}$	10.6±0.2	55
BCl_3^+	12.0±0.5	60
BCl_3^+	12.03±0.02	31
$B^{10}Cl_2^{37+}$	12.0±0.2	55
$B^{11}Cl_2^{35+}$	11.8±0.2	55
BCl_2^+	13.2±0.5	60
BCl_2^+	13.01±0.02	31
$B^{10}Cl^{35+}$	20.0±0.2	55
$B^{11}Cl^{35+}$	17.2±0.2	55
BCl^+	19.2±0.5	60
BCl^+	18.54±0.07	31
B^{11+}	19.5±0.2	55
B^{10+}	20.8±0.2	55
B^+	19.5±1.0	79
B^+	22.5±0.5	60
B^+	13.6±0.2	31
B^+	18.4±0.2	31
B^+	22.35±0.06	31
Cl^+	12.9±0.15	31
Cl^+	17.1±0.15	31
Cl_2^+	12.03±0.05	31
BCl_2^{++}	33.77±0.07	31

[a]See also Table 2.

TABLE 6. Suggested partial ionization cross sections, $\sigma_{i,partial}(\epsilon)$, for BCl_3 (data digitized from figure of Jiao *et al.* [33])

Electron energy (eV)	$\sigma_{i,partial}(\epsilon)$ (10^{-20} m^2)			
	BCl_2^+	BCl_3^+	BCl^+	Cl^+
13.0	0.6	0.6		
15.0	1.7	0.9		
17.0	2.9	1.3		
19.0	4.4	1.6		
21.0	5.1	1.7	0.2	
23.0	5.1	1.6	0.4	0.2
25.0	5.5	1.7	0.6	0.2
27.0	5.5	1.6	0.8	0.4
29.0	5.4	1.6	0.8	0.5

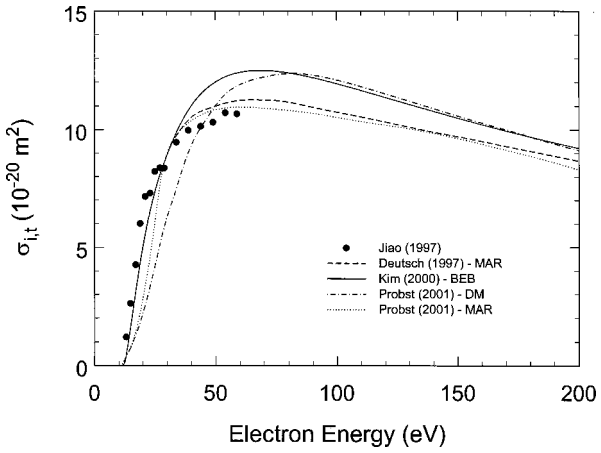

FIG. 9. Total ionization cross section, $\sigma_{i,t}(\epsilon)$, for BCl_3: (●) experimental values (sum of the partial ionization cross sections in Fig. 8 and Table 7) from Ref. 33; (— — —) calculated values/MAR from Ref. 84); (——) calculated values/BEB from Ref. 86; (—·—·—·—) calculated values/DM from Ref. 85; (···) calculated values/MAR from Ref. 85.

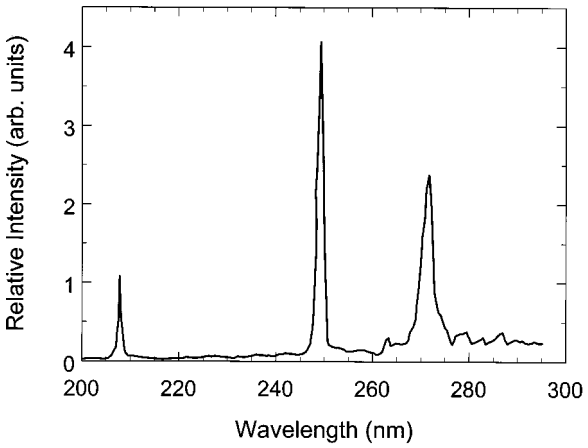

FIG. 10. Emission spectrum between 200 and 300 nm induced by impact of 200 eV electrons on BCl_3 (see text) from Ref. 39.

tion to the emissions from the three species just mentioned, Tokue *et al.*[40] observed two continuous emissions in the wavelength regions 230–380 nm and 400–580 nm which they attributed to BCl_2^*.

Figure 12(a) shows the fluorescence cross section, and Fig. 12(b) the fluorescence quantum yield, of BCl_3 in the wavelength range 106–190 nm as measured by Suto *et al.*[44] using synchrotron light. The fluorescence cross section measurements have a quoted uncertainty of ±30%. They indicate a fluorescence threshold of ~173 nm (7.17 eV) and a number of emission bands in the VIS and the UV regions attributed by Suto *et al.* to excited states of the BCl_2 photofragment. The fluorescence quantum yield was calculated from the ratio of the fluorescence and absorption cross sections [see Figs. 12(a) and 1]. It shows three broad bands with peaks near 118, 130, and 142 nm, which indicate that the dissociating states have, respectively, vertical excitation energies of 10.5, 9.5, and 8.7 eV.

Lee *et al.*[45] extended these room-temperature investigations to excitation wavelengths in the region 45–106 nm. Their fluorescence data are also shown in Figs. 12(a) and 12(b) and have a quoted uncertainty of ±30%. The observed emissions at excitation wavelengths longer than 96 nm were attributed to BCl_2^* and those at excitation wavelengths shorter than 97.5 nm to $BCl^*(A-X)$.[45] Emissions at the thresholds of 88 and 81 nm were attributed to BCl_3^+* and emissions appearing in the 48–64 nm region to B* atoms.

Synchrotron light was also used by Boyle *et al.*[49] to study the fluorescence processes in BCl_3 following vacuum UV (VUV) photoexcitation of BCl_3 in the energy range 9–(137.7 nm) to 22 eV (56.4 nm). Photoexcitation of BCl_3 in this energy range resulted in complicated fluorescence spectra in which the observed emissions were assigned to BCl_2^*, BCl*,

TABLE 7. Suggested total ionization cross sections, $\sigma_{i,t}(\epsilon)$, for BCl_3 for electron energies less than 30 eV (data digitized from figure of Jiao *et al.*[33])

Electron energy (eV)	$\sigma_{i,t}(\epsilon)$ (10^{-20} m^2)
13.0	1.2
15.0	2.6
17.0	4.2
19.0	6.0
21.0	7.0
23.0	7.3
24.0	8.0
27.0	8.3
29.0	8.3

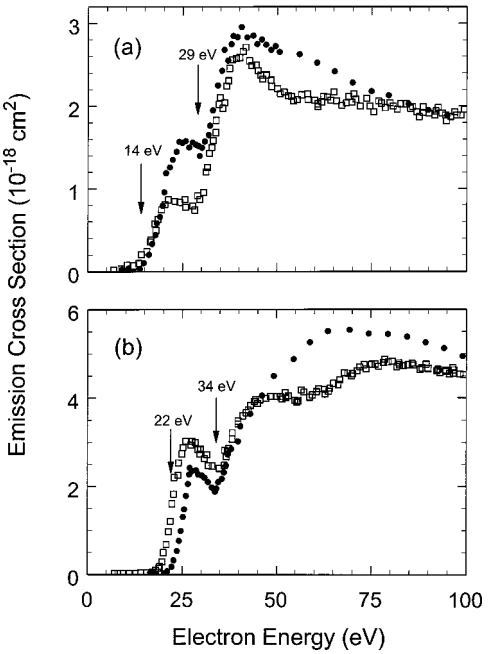

FIG. 11. (a) Emission cross section for the BCl* $A\,^1\Pi \rightarrow X\,^1\Sigma^+$ band as a function of the electron energy: (●) Gilbert *et al.*;[39] (□) Tokue *et al.*[40] (b) Emission cross section for the transition B* $2s\,^2S \rightarrow 2p\,^2P^0$ as a function of the electron energy: (●) Gilbert *et al.*;[39] (□) Tokue *et al.*[40]

TABLE 8. Energies and threshold wavelengths for the dissociation and ionization of BCl_3 as calculated by Lee *et al.*[45]

Process	Energy (eV)	Wavelength (nm)
Dissociation		
BCl_2+Cl	4.61	
$BCl+Cl_2$	5.65	
$BCl+2Cl$	8.16	
$BCl^*(A)+Cl_2$	10.21	121.4
$BCl^*(A)+2Cl$	12.72	97.5
$BCl_2+Cl^*(4P'\ ^2P^0)$	16.31	76.0
$B+3Cl$	13.77	
$B^*(3s\ ^2S)+3Cl$	18.73	66.2
$B^*(2p^2\ ^2D)+3Cl$	19.70	62.9
Ionization		
$BCl_3^+(\tilde{X}\ ^2A_2')+e$	11.64	106.5
$BCl_3^{+*}(\tilde{A}\ ^2E'')+e$	12.19	101.7
BCl_2^++Cl	12.30	
$BCl_3^+(\tilde{B}\ ^2E')+e$	12.66	97.9
$BCl_3^{+*}(\tilde{C}\ ^2A_2'')+e$	14.22	87.2
$BCl_3^{+*}(\tilde{D}\ ^2E')+e$	15.32	80.9
$BCl_3^{+*}(\tilde{E}\ ^2A_1')+e$	17.74	69.9
$BCl^++2Cl+e$	18.37	

BCl_3^{+*}, BCl_2^{+*}, and B*. As the authors noted, their experiments are sensitive to those Rydberg states of BCl_3 which photodissociate to an excited state of a neutral fragment that fluoresces, and to valence states of the parent or a fragment ion that fluoresce. These two processes can be represented as[49]

$$BCl_3+h\nu_1\rightarrow BCl_3^*, \tag{5a}$$

$$BCl_3^*\rightarrow BCl_2^*+Cl, \tag{5b}$$

$$BCl_3^*\rightarrow BCl^*+(Cl_2\ \text{or}\ 2Cl), \tag{5c}$$

$$BCl_3^*\rightarrow B^*+(3Cl\ \text{or}\ Cl_2+Cl), \tag{5d}$$

$$BCl_2^*\ \text{or}\ BCl^*\ \text{or}\ B^*\rightarrow BCl_2\ \text{or}\ BCl\ \text{or}\ B+h\nu_2, \tag{5e}$$

and

$$BCl_3+h\nu_1\rightarrow BCl_3^{+*}+e, \tag{6a}$$

$$BCl_3^{+*}\rightarrow BCl_3^++h\nu_2, \tag{6b}$$

$$BCl_3^{+*}\rightarrow BCl_2^{+*}+Cl\rightarrow BCl_2+Cl+h\nu_2, \tag{6c}$$

where $h\nu_1$ and $h\nu_2$ represent, respectively, photons in the VUV (50–150 nm) and UV/VIS (200–700 nm).

Finally, a number of spectroscopic studies have been performed on discharges in gas mixtures containing BCl_3 (e.g., see Refs. 88–90 for mixtures of BCl_3 with N_2 or Ar), which provided additional information regarding the dissociation products of BCl_3 and the role of metastable states of the buffer gas employed. Thus, Breitbarth[88] concluded that in BCl_3/N_2 discharges, direct electron-impact excitation is not responsible for the observed BCl* and B* emissions, but rather an energy transfer from the $N_2^*(W)$ state to the BCl_x species present in his system. In the case of BCl_3/Ar discharges, Scheller *et al.*[89] argued that argon metastables indirectly enhance molecular dissociation by increasing the positive ion density via Penning ionization (that is, especially at concentrations below 5%, Penning ionization generates BCl_3^+ which subsequently undergoes dissociative recombination). Similarly, Breitbarth and Ducke[90] observed three broad emissions with maxima at 305, 350, and 480 nm in rf discharges using pure BCl_3. They attributed all three emissions to the electronically excited BCl_2^* fragment. In discharges with pure BCl_3, they showed the dominant process for formation of excited $BCl^*(A)$ fragments to be direct electron-impact excitation of $BCl(X)$. For mixtures of BCl_3/Ar, however, the $BCl^*(A\ ^1\Pi)$ species are also produced via energy transfer from argon metastables.

It should perhaps be mentioned that a number of other

TABLE 9. Calculated and observed minimum energies for the electron-impact-induced fragmentation of BCl_3 into excited boron (B*), boron chloride (BCl*), and BCl_2^* fragments

Fragments[a]	Minimum energy (eV)	Reference
$B^*(3s\ ^2S)+Cl_2+Cl$	[16.2][b]	39
	[16.28]	40
$B^*(3s\ ^2S)+3Cl$	[18.70]	40
	[18.8]	39
	22.0±1.5[c]	39
$B^*(3s\ ^2S)+Cl_2+Cl^+$	[29.1]	39
$B^*(3s\ ^2S)+2Cl+Cl^+$	[31.7]	39
$B^*(2p^2\ ^2D)+Cl_2+Cl$	[17.1]	39
	[17.25]	40
	17.7±0.2	40
$B^*(2p^2\ ^2D)+3Cl$	[19.67]	40
	[19.7]	39
	20.0±0.5	40
$B^*(2p^2\ ^2D)+Cl_2+Cl^+$	[30.0]	39
	[30.28]	40
$B^*(2p^2\ ^2D)+2Cl+Cl^+$	[32.6]	39
	[32.70]	40
$B^*(3p\ ^2P^0)+Cl_2+Cl$	[17.34]	40
	17.7±0.4	40
$B^*(3p\ ^2P^0)+3Cl$	[19.76]	40
	19.7±0.3	40
$B^*(3p\ ^2P^0)+Cl_2+Cl^+$	[30.37]	40
$B^*(3p\ ^2P^0)+2Cl+Cl^+$	[32.79]	40
$BCl^*(A\ ^1\Pi)+Cl_2$	[10.50]	39,40
$BCl^*(A\ ^1\Pi)+2Cl$	[13.1]	39
	[12.92]	40
	13.9±0.5	40
	14.0±1.5	39
$BCl^*(A\ ^1\Pi)+Cl+Cl^+$	[26.0]	39
	[25.95]	40
	25–29	40
	29.0±2.0	39
$BCl_2^*(468\ \text{nm})+Cl$	[6.75]	40
	7.0±0.6	40
	7.17	44
$BCl_2^*(330\ \text{nm})+Cl$	[8.90]	40
	9.4±0.4	40
	9.80	44

[a]Excited fragments are designated by the asterisk (*).
[b]Values in brackets are calculated by the respective authors using the enthalpies of formation for the parent molecule, the related fragments, and electronic energies of the excited states involved (see respective references for details).
[c]Values not in brackets are measurements.

TABLE 10. Absolute cross sections of boron and boron chloride fragment emissions formed by 100 eV electrons impacting on BCl_3, and associated wavelengths, transitions, and measured onsets

Fragment	Wavelength (nm)	Transition	Cross section (10^{-18} cm^2)	Onset energy (eV)	Reference
Boron	208.9	$2p^2\,^2D \rightarrow 2p\,^2P^0$	1.8±0.9[a]	23.0±1.5	39
				34.5±2.0	39
	208.9	$2p^2\,^2D \rightarrow 2p\,^2P^0$	4.9±1.0		40
Boron	249.8	$3s\,^2S \rightarrow 2p\,^2P^0$	4.9±1.6	22.0±1.5	39
				34.0±2.0	39
	249.7	$3s\,^2S \rightarrow 2p\,^2P^0$	4.5±0.7		40
Boron chloride	272.4[b]	$A\,^1\Pi \rightarrow X\,^1\Sigma^+$	1.9±0.4	14.0±1.5	39
				29.0±2.0	39
	271.5[c]	$A\,^1\Pi \rightarrow X\,^1\Sigma^+$	1.9±0.3		40

[a]Estimated uncertainty ±50%.
[b]The wavelength refers to the location of the maximum intensity of the $\Delta\nu=0$ vibrational sequence of the $A\,^1\Pi \rightarrow X\,^1\Sigma^+$ band.
[c]Unresolved (0,0), (1,1), and (2,2) bands.

photophysical studies have been made to probe the properties of BCl_3 gas discharges. Discharges containing BCl_3 provide a convenient source of BCl radicals whose Stark-mixed laser-induced fluorescence spectrum can be used to determine the magnitude of the sheath electric field with high spatial and temporal resolution.[91] For instance, Gottscho[92] used Stark-mixed laser-induced fluorescence to measure space–time-resolved maps of sheath electric fields in discharges through BCl_3 and in mixtures of BCl_3 with Ar as a function of power density (0.14–0.41 W cm^{-3}) and frequency (dc to 10 MHz).

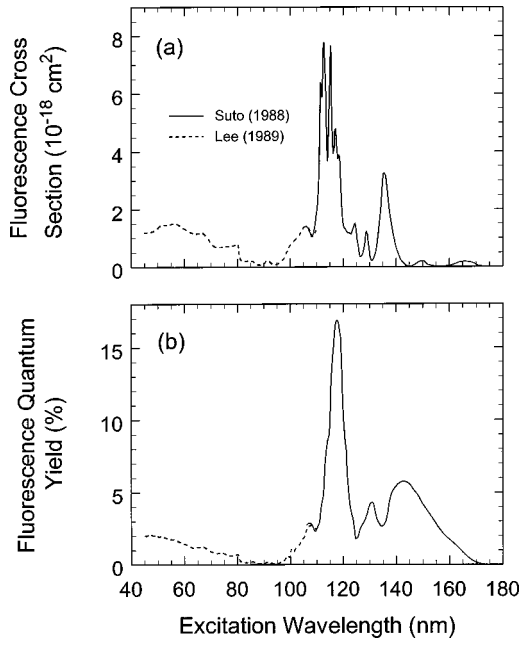

FIG. 12. (a) Fluorescence cross section and (b) fluorescence quantum yield as a function of excitation wavelength for BCl_3: (——) Ref. 44; (- - -) Ref. 45.

5. Electron Attachment

Electron attachment to BCl_3 has been experimentally investigated using electron beam[31–34,36,37] and electron swarm[61,93] methods. There have also been some studies of negative ion formation in BCl_3 gas discharges.[65,94,95] The results of these investigations are synthesized, assessed, and discussed in this section.

5.1. Electron Attachment Processes in BCl_3

Collectively, the results of a number of electron-beam mass spectrometric studies[31–33,36,37] on the relative cross sections for the production of fragment negative ions by low-energy electron impact on BCl_3, are consistent with the reactions

$$BCl_3 + e \rightarrow BCl_3^{-*} \rightarrow BCl_2 + Cl^-, \quad (7)$$

$$BCl_3 + e \rightarrow BCl_3^{-*} \rightarrow BCl + Cl_2^-, \quad (8)$$

and

$$BCl_3 + e \rightarrow BCl_3^{-*} \ (\text{long lived}). \quad (9)$$

They all show that dissociative electron attachment to BCl_3 produces primarily Cl^- via Reaction (7). These studies[32,33,36,37] also showed the production of Cl_2^- via Reaction (8) albeit with much smaller probability (the amount of Cl_2^- ions may be affected by ion–molecule reactions[33]). The existence of long lived BCl_3^{-*} ions [Reaction (9)] at thermal electron energies has been indicated by electron beam[36,37] and by electron swarm studies (see later in this section). These findings are discussed further below.

The dissociative electron attachment Reaction (7) is endoergic by ~1 eV. Olthoff[36] estimated the energy threshold for Cl^- to be ~0.7 eV from thermodynamic data, and Baeck and Bartlett[29] calculated the dissociation energy of BCl_3^- into $BCl_2 + Cl^-$ to be ~1.59 eV. In accord with these values, Stockdale *et al.*[32] found the lowest peak in the relative cross

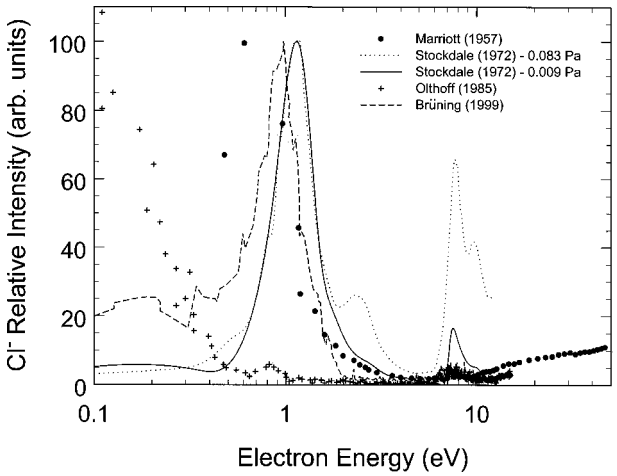

FIG. 13. Relative cross section for the production of Cl^- by electron impact on BCl_3: (●) Ref. 31; (···) Ref. 32 for two pressures (0.009 and 0.083 Pa) showing the production of Cl^- directly via Reaction (7) at 1.1 eV and indirectly via Reactions (10a) and (10b) at higher energies (see text); (+) Ref. 36 under single-collision conditions; (— — —) Ref. 37 at a pressure of ~0.001 Pa.

section for the formation of Cl^- from BCl_3 to be located at (1.1 ± 0.1) eV, and Brüning[37] observed the most intense peak in the Cl^- production to be at ~0.9 eV (Fig. 13). However, in similar studies Olthoff[36] found the cross section for Cl^- to peak at an energy (Fig. 13) well below the thermodynamic threshold of 0.7 eV. Although the production of Cl^- is expected to be temperature dependent[96]—and thus possible differences in the temperature of the various experimental studies may influence the magnitude and position of the low-energy Cl^- resonance—the temperature in these experiments is not expected to differ appreciably. Brüning, for instance, quotes the temperature of his experiment to be ~340 K, and the temperature in the experiment of Olthoff is expected to be similar. Nonetheless, a study of the effect of temperature on the cross section for the production of Cl^- ions is indicated for this molecule. The observation of Cl^- may also be attributed to impurities produced by reactions of the BCl_3 with the gas manifold walls.

Besides the Cl^- peak near 1 eV, the relative cross section for the production of Cl^- from BCl_3 was found[32,36,37] to have a number of weaker peaks between 6 and 10 eV (see Fig. 13 and Table 3) which are near the location of electron-excited Feshbach resonances observed in electron transmission studies.[30] Since the pressure in the experiments of Brüning[37] and Olthoff[36] was sufficiently low (on the order of 10^{-5} mbar) to ensure single-collision conditions, the Cl^- observed in these investigations between 6 and 10 eV is due to primary processes, that is, due to the decay of the negative ion states in this energy range via dissociative electron attachment. However, in the experiments of Stockdale *et al.*[32] the pressure was much higher—$(9.2—82)\times10^{-5}$ mbar—and in this case, in addition to the 1.1 eV peak, Stockdale *et al.* observed Cl^- peaks around 2.5 and 8 eV. The intensity of these peaks varied as the square of the BCl_3 pressure. They were attributed[32] to the processes

$$e+BCl_3\rightarrow BCl_3^*+e_{slow}, \tag{10a}$$

$$e_{slow}+BCl_3\rightarrow Cl^-+BCl_2, \tag{10b}$$

which is due to the production of Cl^- by dissociative attachment to BCl_3 of electrons, e_{slow}, that have first been slowed down to near 1 eV via the negative ion states near 2.5 eV and 8 eV.

In addition, the measurements of Marriott and Graggs[31] shown in Fig. 13 indicate the production of Cl^- at energies $\gtrsim$9 eV, which may be due to the ion-pair process $BCl_3+e\rightarrow BCl_2^++Cl^-+e$. Marriott and Graggs were careful to point out however that because BCl_3 hydrolyzes readily ($BCl_3+3H_2O\rightarrow H_3BO_3+3HCl$), the production of HCl may affect the measurements dealing with the products Cl^-, Cl^+, and Cl^{++} which may originate from electron impact on HCl.

The dissociative electron attachment Reaction (8) is also endoergic. Olthoff[36] estimated the threshold energy for Reaction (8) to be ~3.3 eV, and Baeck and Bartlett[29] calculated the dissociation energy of BCl_3^- into $BCl+Cl_2^-$ to be 4.01 eV. These values are incompatible with the observation by Stockdale *et al.*[32] that the relative cross section of Cl_2^- ions from BCl_3 peaks at 1.1 ± 0.1 eV and the observations by Olthoff[36] and Brüning[37] that the relative cross section for the production of Cl_2^- ions from BCl_3 peaks near 0.0 eV. Indeed, because of this discrepancy, the observed Cl_2^- signals in these experiments may be due to impurities. Interestingly, Brüning observed BCl_4^-, which Jiao *et al.*[33] found to be an ion–molecule reaction product resulting from the rapid reaction of Cl_2^- with BCl_3. No BCl_2^- or BCl^- fragment negative ions were reported in any of these studies.

Reaction (9) occurs at thermal and near-thermal energies. The transient BCl_3^-* species, which is initially formed by electron capture, is metastable and thus, can decay by autodetachment. It is, however, long lived.[36,37,65,93] Its autodetachment lifetime was inferred[36] to be at least 60 μs at thermal energies and temperatures somewhat higher than ambient (due to the heating of the gas from the hot filament in these experiments). This long lifetime may result from the fact that the equilibrium geometries of BCl_3 and BCl_3^- are different—the BCl_3 molecule is planar (D_{3h}) and the BCl_3^- ion is pyramidal (C_{3v}) (Sec. 2). Such geometrical changes are known to lead to long lifetimes for a number of transient anions.[97] The long-lived BCl_3^-* ion can rid itself of its extra energy by collision (or radiation) and lead to the formation of a stable parent negative ion BCl_3^- since the BCl_3 molecule has a positive electron affinity (Table 3). The electron attachment rate constants measured in swarm experiments (Sec. 5.3) at low E/N may thus be due to Reaction (9). They may be sensitive to the gas temperature (decrease with increasing gas temperature above ambient) since the electron affinity of BCl_3 is small (Table 3) and the probability of thermally induced electron detachment from the stabilized BCl_3^- ($BCl_3^-+\text{heat}\rightarrow BCl_3+e$) can be large.[98]

A summary of the data on negative ions found in electron beam studies produced by low-energy electron impact on BCl_3 is given in Table 3 (see also Fig. 2).

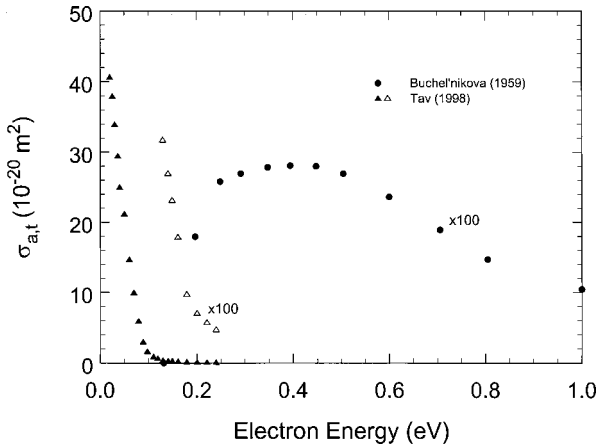

FIG. 14. Total electron attachment cross section as a function of electron energy, $\sigma_{a,t}(\epsilon)$, for BCl_3: (●) electron beam data from Ref. 34 (Note that these data have been multiplied by a factor of 100 for the convenience of display); (▲) electron swarm data from Ref. 61 (the data shown with open triangles are multiplied by 100 to facilitate comparison).

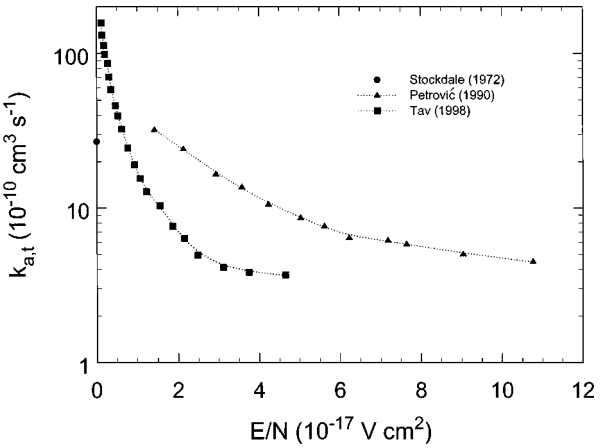

FIG. 15. Total electron attachment rate constant as a function of E/N, $k_{a,t}(E/N)$, for BCl_3: (▲) Ref. 93; (■) Ref. 61; (●) thermal value from Ref. 32.

5.2. Total Electron Attachment Cross Section as a Function of Electron Energy, $\sigma_{a,t}(\epsilon)$

There has been only one measurement of the total electron attachment cross section, $\sigma_{a,t}(\epsilon)$, of BCl_3 using the electron beam method, namely, that by Buche'nikova.[34] This total electron attachment cross section is shown in Fig. 14. It has a maximum at near 0.4 eV and a cross section value at this energy of 2.8×10^{-17} cm^2. While Buche'nikova's technique yields total electron attachment values, the data in Fig. 14 were attributed to the production of Cl^- via Reaction (7). As has been found for other molecules that Buchel'nikova had investigated, his cross section data for BCl_3 are considered to be lower than their true values.

5.3. Total Electron Attachment Rate Constant, $k_{a,t}$, as a Function E/N and $\langle\epsilon\rangle$

There have been two[61,93] investigations of electron attachment to BCl_3 using the electron swarm method. Both of these studies employed mixtures of BCl_3 with N_2 and were conducted at room temperature (~295 K). In both studies the total electron attachment rate constant, $k_{a,t}(E/N)$, was measured as a function of the density-reduced electric field E/N. These measurements are compared in Fig. 15. The measurements of Petrović *et al.*[93] have a quoted uncertainty of ±30%. Although Tav *et al.*[61] gave no uncertainty for their measurements, the uncertainty in their measurements is expected to be at least as large as that of Petrović *et al.*[93] considering the large variation of their data with time following the introduction of BCl_3 into their reaction chamber. Also shown in Fig. 15 is an earlier measurement[32] (see Fig. 15 and Sec. 5.4) of the thermal electron attachment rate constant. There are substantial differences between these data, stressing the need for new measurements.

Petrović *et al.*[93] argued that since the threshold for dissociative electron attachment producing either Cl^- or Cl_2^- is greater than ~1 eV and since for the E/N range they investigated the values of the mean electron energy are less than ~1 eV, the electron attachment rate constants they measured in their experiments (Fig. 15) are due to the formation of BCl_3^-. This interpretation would be consistent with the mass spectrometric observation[36,37] of long lived BCl_3^-*, and with the conclusion of Gottscho and Gaebe[65] that BCl_3^- is the dominant negative ion formed in rf discharges using pure BCl_3. Although Petrović *et al.* observed only Cl^- in dc discharges of BCl_3, they argued that the difference between the results of the dc and rf discharge studies may be due to the difference in the electron energies in the types of discharges. In DC discharges the mean electron energies may be too high to enable production of BCl_3^-, in contrast to the bulk of rf plasma where the electron energies are much lower (see also Ref. 65).

Similarly, Tav *et al.*[61] attributed the total electron attachment rate constant they measured at low electron energies (≲0.1 eV) to the formation of BCl_3^-, and the weaker electron attachment at higher energies to Cl^- formation. However, neither in the study of Petrović *et al.*[93] nor in the study of Tav *et al.* were the negative ions directly identified. It is emphasized that this indirect inference of the identity of the ions needs further scrutiny. The argument, for instance, that Cl^- cannot be formed at low energies for energetic reasons may not be correct, if there is a large effect of temperature on the dissociative electron attachment process generating Cl^-. Also, since the electron affinity of the BCl_3 molecule is small (Table 3), the electron may be detached thermally from the stabilized BCl_3^- ion at temperatures at and above ambient. Therefore, to fully characterize the electron attachment processes for this molecule, an investigation is needed of the temperature dependence of the formation of both Cl^- and BCl_3^-.

The $k_{a,t}(E/N)$ data in Fig. 15 are plotted in Fig. 16 as a function of the mean electron energy, $\langle\epsilon\rangle$, using the $\langle\epsilon\rangle$ (E/N) data for $N_2(T=300\,\mathrm{K})$ given in Table A.II of Christophorou and Olthoff.[96]

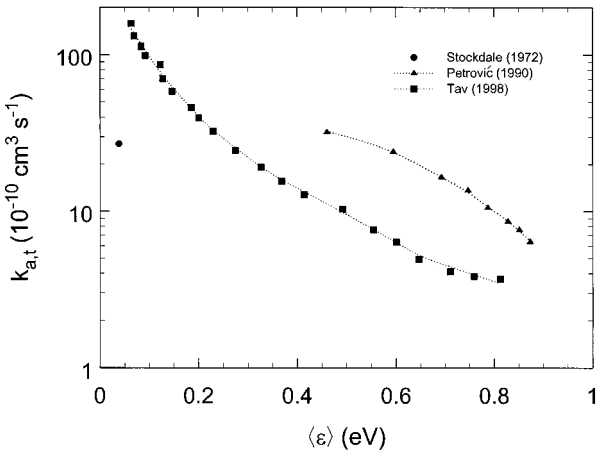

FIG. 16. Total electron attachment rate constant as a function of the mean electron energy $\langle\epsilon\rangle$, $k_{a,t}(\langle\epsilon\rangle)$, for BCl_3: (▲) Ref. 93; (■) Ref. 61; (●) thermal value from Ref. 32.

5.4. Thermal Electron Attachment Rate Constant, $(k_{a,t})_{th}$

The thermal ($T \cong 295$ K) value, $(k_{a,t})_{th}$, of the total electron attachment rate constant of BCl_3 has been measured by Stockdale *et al.*[32] to be 2.7×10^{-9} cm^3 s^{-1}.

5.5. Swarm-Unfolded Total Electron Attachment Cross Section, $\sigma_{a,t}(\epsilon)$

Tav *et al.*[61] unfolded the total electron attachment cross section $\sigma_{a,t}(\epsilon)$ shown in Fig. 14 from their data on $k_{a,t}(E/N)$ and the known electron energy distribution functions in the buffer gas N_2. They attributed the rise in the cross section below ~0.1 eV to the formation of BCl_3^-. The smaller cross section at higher energies was attributed to Cl^- formation, but no direct identification of the negative ions was obtained. They indicated that their derived cross section has an uncertainty of ±20%, but the uncertainty is probably much larger than indicated. The disagreement between the swarm-unfolded total electron attachment cross section[61] and the beam-determined values[34] is large. Clearly, there is a need for further measurements.

5.6. Negative Ion Photodetachment in BCl_3 Plasmas

Gaebe *et al.*[94] described a spectroscopic diagnostic technique that provides the response of a radio-frequency discharge to electrons photodetached from negative ions in BCl_3. In this technique the spatially and temporally resolved charges in the local electric field of a 50 kHz discharge through BCl_3 (changes in the local electric field which resulted from photodetachment of electrons from negative ions) are monitored using Stark-mixing spectroscopy (e.g., see Refs. 91,99).

Similarly, Fleddermann and Hebner[95] investigated the Cl^- concentration and the electron density in BCl_3-containing inductively coupled plasmas using laser light to photodetach

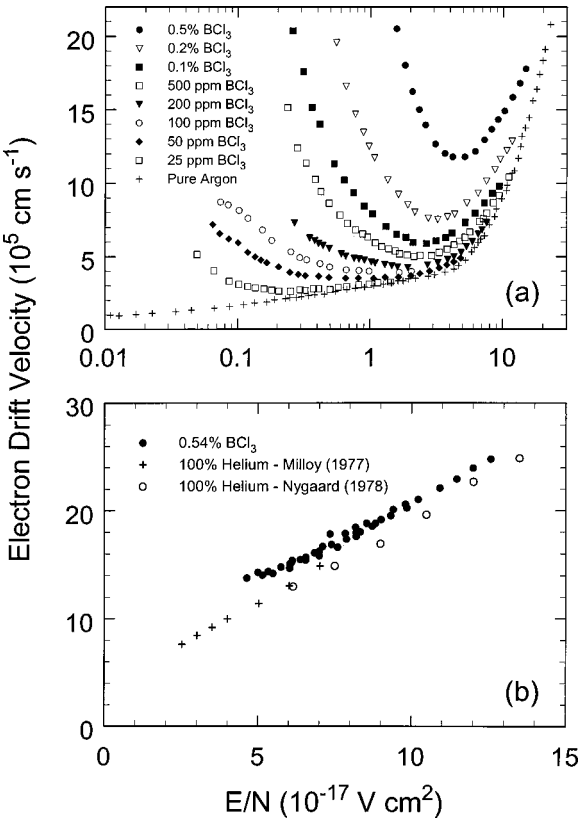

FIG. 17. (a) Electron drift velocity as a function of E/N, $w(E/N)$, for mixtures of BCl_3 in argon (data of Mosteller *et al.* from Ref. 14). (b) Electron drift velocity as a function of E/N, $w(E/N)$, for a 0.54% BCl_3 mixture with He [(●) Ref. 14], in comparison with the $w(E/N)$ for pure He [(+) Ref. 100; (○) Ref. 101].

electrons from Cl^- ions. They detected the photodetached electrons and the steady-state electron density using a microwave interferometer, which allowed measurement of absolute negative ion densities as a function of gas mixture and reactor parameters. The 266 nm radiation from a frequency-quadrupled Nd:yttrium–aluminum–garnet laser was used for photodetachment. The plasma was probed at lower photon energy (355 nm) to photodetach electrons from other possible negative ions present in the plasma. To within the sensitivity of their measurement (1.3×10^8 cm^{-3}), no other negative ions (such as BCl_x^- or Cl_2^-) were detected.

6. Electron Transport Coefficients

There are no measurements of the electron transport coefficients in pure BCl_3. However, there have been some measurements of the electron drift velocity, $w(E/N)$, in BCl_3/Ar gas mixtures at concentrations of BCl_3 in Ar ranging from 2.5×10^{-5} to 5×10^{-3}, which are representative of those used in plasma applications.[14] According to Mosteller *et al.*,[14] these mixtures exhibit strong electron attachment at low E/N, and the $w(E/N)$ measurements [shown in Fig. 17(a)] show regions of negative differential conductivity. Mosteller *et al.* also measured the $w(E/N)$ in a mixture of 0.54% BCl_3 in He. These measurements are shown in Fig.

17(b), where they are compared with the $w(E/N)$ of Milloy and Crompton[100] and Nygaard *et al.*[101] for pure He.

7. Suggested and Needed Data

The only suggested electron collision data are those for $\sigma_{i,t}(\epsilon)$ (Fig. 9; Table 7). There is a need for further measurements of this cross section, and also for measurements of the cross sections of all other principal electron scattering processes for this molecule. Measurements are also needed of the electron transport, ionization, and attachment coefficients in pure BCl_3 and in mixtures.

8. Acknowledgments

We wish to thank Professor E. Illenberger for providing us with parts of Dr. F. Brüning's dissertation and Professor M. Hayashi for making available to us his literature list on BCl_3.

9. References

[1] D. L. Flamm and V. M. Donnelly, Plasma Chem. Plasma Process. **1**, 317 (1981).
[2] R. J. Saia and B. Gorowitz, Solid State Technol., April, 247 (1983).
[3] G. J. Sonek and J. M. Ballantyryne, J. Vac. Sci. Technol. B **2**, 653 (1984).
[4] R. A. Morgan, *Plasma Etching in Semiconductor Fabrication* (Elsevier, Amsterdam, 1985).
[5] *Application of Plasma Processes to VLSI Technology*, edited by T. Sugano (Wiley-Interscience, New York, 1985).
[6] S. S. Cooperman, H. K. Choi, H. H. Sawin, and D. F. Kolesar, J. Vac. Sci. Technol. B **7**, 41 (1989).
[7] J. W. Lee, J. Hong, E. S. Lambers, C. R. Abernathy, S. J. Pearton, W. S. Hobson, and F. Ren, Plasma Chem. Plasma Process. **17**, 155 (1997).
[8] J. W. Coburn, Plasma Chem. Plasma Process. **2**, 1 (1982).
[9] S. J. Pearton, W. S. Hobson, C. R. Abernathy, F. Ren, T. R. Fullowan, A. Katz, and A. P. Perley, Plasma Chem. Plasma Process. **13**, 311 (1993).
[10] J. W. Lee, J. Hong, E. S. Lambers, C. R. Abernathy, S. J. Pearton, W. S. Hobson, and F. Ren, Plasma Chem. Plasma Process. **17**, 169 (1997).
[11] J. Hong, H. Cho, T. Maeda, C. R. Abernathy, S. J. Pearton, R. J. Shul, and W. S. Hobson, J. Vac. Sci. Technol. B **16**, 2690 (1998).
[12] E. Meeks, P. Ho, A. Ting, and R. J. Buss, J. Vac. Sci. Technol. A **16**, 2227 (1998).
[13] J. Hong, J. A. Caballero, E. S. Lambers, J. R. Childress, and S. J. Pearton, J. Vac. Sci. Technol. B **16**, 3349 (1998).
[14] D. L. Mosteller, Jr., M. L. Andrews, J. D. Clark, and A. Garscadden, J. Appl. Phys. **74**, 2247 (1993).
[15] V. McKoy, C. Winstead, and W. L. Morgan, Data Compilation for Plasma Chemistries, Technology Transfer No. 97043274A-TR, Sematech, August 22, 1997 (data quoted by Sematech's permission).
[16] L. G. Christophorou, J. K. Olthoff, and M. V. V. S. Rao, J. Phys. Chem. Ref. Data **25**, 1341 (1996) (Electron Interactions with CF_4).
[17] L. G. Christophorou, J. K. Olthoff, and M. V. V. S. Rao, J. Phys. Chem. Ref. Data **26**, 1 (1997) (Electron Interactions with CHF_3).
[18] L. G. Christophorou, J. K. Olthoff, and Y. Wang, J. Phys. Chem. Ref. Data **26**, 1205 (1997) (Electron Interactions with CCl_2F_2).
[19] L. G. Christophorou and J. K. Olthoff, J. Phys. Chem. Ref. Data **27**, 1 (1998) (Electron Interactions with C_2F_6).
[20] L. G. Christophorou and J. K. Olthoff, J. Phys. Chem. Ref. Data **27**, 889 (1998) (Electron Interactions with C_3F_8).
[21] L. G. Christophorou and J. K. Olthoff, J. Phys. Chem. Ref. Data **28**, 131 (1999) (Electron Interactions with Cl_2).
[22] L. G. Christophorou and J. K. Olthoff, J. Phys. Chem. Ref. Data **28**, 967 (1999) (Electron Interactions with Plasma Processing Gases: An Update for CF_4, CHF_3, C_2F_6, and C_3F_8).
[23] L. G. Christophorou and J. K. Olthoff, J. Phys. Chem. Ref. Data **29**, 267 (2000) (Electron Interactions with SF_6).
[24] L. G. Christophorou and J. K. Olthoff, J. Phys. Chem. Ref. Data **29**, 553 (2000) (Electron Interactions with CF_3I).
[25] L. G. Christophorou and J. K. Olthoff, J. Phys. Chem. Ref. Data **30**, 449 (2001) (Electron Interactions with c-C_4F_8).
[26] G. Herzberg, *Molecular Spectra and Molecular Structure II: Infrared and Raman Spectra of Polyatomic Molecules* (Van Nostrand Reinhold, New York, 1945), p. 302.
[27] K. Ueda, H. Chiba, Y. Sato, T. Hayashi, E. Shigemasa, and A. Yagishita, J. Chem. Phys. **101**, 7320 (1994).
[28] L. G. Shpinkova, D. M. P. Holland, and D. A. Shaw, Mol. Phys. **96**, 323 (1999).
[29] K. K. Baeck and R. J. Bartlett, J. Chem. Phys. **106**, 4604 (1997).
[30] J. A. Tossell, J. H. Moore, and J. K. Olthoff, Intern. J. Quantum Chem. **XXIX**, 1117 (1986).
[31] J. Marriott and J. D. Craggs, J. Electron. Control **3**, 194 (1957).
[32] J. A. Stockdale, D. R. Nelson, F. J. Davis, and R. N. Compton, J. Chem. Phys. **56**, 3336 (1972).
[33] C. Q. Jiao, R. Nagpal, and P. Haaland, Chem. Phys. Lett. **265**, 239 (1997).
[34] I. S. Buchel'nikova, Sov. Phys. JETP **35**, 783 (1959).
[35] E. W. Rothe, B. P. Mathur, and G. P. Reck, Inorg. Chem. **19**, 829 (1980).
[36] J. K. Olthoff, Ph.D. dissertation, University of Maryland, 1985.
[37] F. Brüning, Ph.D. dissertation, Freie Universität Berlin, 1999.
[38] Z. J. Jabbour, K. E. Martus, and K. Becker, Z. Phys. D: At. Mol. Clusters **9**, 263 (1988).
[39] P. G. Gilbert, R. B. Siegel, and K. Becker, Phys. Rev. A **41**, 5594 (1990).
[40] I. Tokue, M. Kudo, M. Kusakabe, T. Honda, and Y. Ito, J. Chem. Phys. **96**, 8889 (1992).
[41] P. J. Bassett and D. R. Lloyd, J. Chem. Soc. A, 1551 (1971).
[42] H. Biehl, K. J. Boyle, D. M. Smith, R. P. Tuckett, K. R. Yoxall, K. Codling, P. A. Hatherly, and M. Stankiewicz, J. Chem. Soc., Faraday Trans. **92**, 185 (1996).
[43] V. H. Dibeler and J. A. Walker, Inorg. Chem. **8**, 50 (1969).
[44] M. Suto, C. Ye, J. C. Han, and L. C. Lee, J. Chem. Phys. **89**, 6653 (1988).
[45] L. C. Lee, J. C. Han, and M. Suto, J. Chem. Phys. **91**, 2036 (1989).
[46] J. C. Creasey, P. A. Hatherly, I. R. Lambert, and R. P. Tuckett, Mol. Phys. **79**, 413 (1993).
[47] S. Georgiou, E. Raptakis, X. Xing, E. Hontzopoulos, and Y. P. Vlahoyannis, J. Chem. Soc. Faraday Trans. **90**, 3633 (1994).
[48] H. Biehl, J. C. Creasey, D. M. Smith, R. P. Tuckett, K. R. Yoxall, H. Baumgärtel, H. W. Jochims, and U. Rockland, J. Chem. Soc. Faraday Trans. **91**, 3073 (1995).
[49] K. J. Boyle, D. P. Seccombe, R. P. Tuckett, H. Baumgärtel, and H. W. Jochims, J. Phys. B **32**, 2569 (1999).
[50] H. J. Maria, J. R. McDonald, and S. P. McGlynn, J. Am. Chem. Soc. **95**, 1050 (1973).
[51] A. A. Planckaert, P. Sauvageau, and C. Sandorfy, Chem. Phys. Lett. **20**, 170 (1973).
[52] A. Slaoui, F. Foulon, C. Fuchs, E. Fogarassy, and P. Siffert, Appl. Phys. A **50**, 317 (1990).
[53] E. Ishiguro, S. Iwata, Y. Suzuki, A. Mikuni, and T. Sasaki, J. Phys. B **15**, 1841 (1982).
[54] M. Cini, F. Maracci, and R. Platania, J. Electron Spectros. Related Phenomena **41**, 37 (1986).
[55] W. S. Koski, J. J. Kaufman, and C. F. Pachucki, J. Am. Chem. Soc. **81**, 1326 (1959).
[56] M. F. Lappert, M. R. Litzow, J. B. Pedley, P. N. K. Riley, T. R. Spalding, and A. Tweedale, J. Chem. Soc. A, 2320 (1970).
[57] H.-O. Berger, J. Kroner, and H. Nöth, Chem. Ber. **109**, 2266 (1976).
[58] D. Goutier and L. A. Burnelle, Chem. Phys. Lett. **18**, 460 (1973).
[59] R. J. Boyd and D. C. Frost, Chem. Phys. Lett. **1**, 649 (1968).
[60] O. Osberghaus, Z. Phys. **128**, 366 (1950).
[61] C. Tav, P. G. Datskos, and L. A. Pinnaduwage, J. Appl. Phys. **84**, 5805 (1998).
[62] W. A. Isaacs, C. W. McCurdy, and T. N. Rescigno, Phys. Rev. A **58**, 2881 (1998).
[63] M. H. F. Bettega, Phys. Rev. A **61**, 042703 (2000).
[64] D. R. Armstrong and P. G. Perkins, J. Chem. Soc. A, 1218 (1967).
[65] R. A. Gottscho and C. E. Gaebe, IEEE Trans. Plasma Science **PS-14**, 92 (1986).

[66] G. Herzberg, *Molecular Spectra and Molecular Structure II: Infrared and Raman Spectra of Polyatomic Molecules* (Van Nostrand Reinhold, New York, 1945), p. 178.
[67] D. R. Stull and H. Prophet, *JANAF Thermochemical Tables*, 2nd ed. (NSRDS-NBS, June 1971), Vol. 37.
[68] L. A. Farrow, J. Chem. Phys. **82**, 3625 (1985).
[69] M. E. Jacox, K. K. Irikura, and W. E. Thompson, J. Chem. Phys. **104**, 8871 (1996).
[70] J. H. Callomon, E. Horota, K. Kuchitsu, W. J. Lafferty, A. G. Maki, and C. S. Pole, in Landolt-Bornstein, *Numerical Data and Functional Relationships in Science and Technology, New Series, Group II Atomic and Molecular Physics*, edited by K. H. Hellwege and A. M. Hellwege (Springer, New York, 1976), Vol. 7.
[71] C. Leibovici, J. Mol. Struct. **14**, 459 (1972).
[72] R. Nagpal and A. Garscadden, Appl. Phys. Lett. **64**, 1626 (1994).
[73] *CRC Handbook of Chemistry and Physics*, 70th ed., edited by R. C. Weast, D. R. Lide, M. J. Astle, and W. H. Beyer (CRC, Boca Raton, FL, 1990), p. E-74.
[74] R. S. Armstrong, M. J. Aroney, A. Hector, and R. J. W. Le Févre, J. Chem. Soc. B, 1203 (1968).
[75] R. I. Keir and G. L. D. Ritchie, Chem. Phys. Lett. **290**, 409 (1998).
[76] K. Iijima and S. Shibata, Bull. Chem. Soc. Jpn. **53**, 1908 (1980).
[77] R. Franzi, M. Geoffroy, E. A. Lucken, and N. Leray, J. Chem. Phys. **78**, 708 (1983).
[78] V. McKoy, C. Winstead, W. L. Morgan, and P. D. Haaland, *Data Compilation for Plasma Chemistries No. 2*, Technology Transfer No. 98063515A-TR (Sematech, June 30, 1998) (data quoted by Sematech's permission).
[79] R. W. Law and J. L. Margrave, J. Chem. Phys. **25**, 1086 (1956).
[80] R. C. Wetzel, F. A. Baiocchi, T. R. Hayes, and R. C. Freund, Phys. Rev. A **35**, 559 (1987).
[81] E. Krishnakumar and S. K. Srivastava, J. Phys. B **21**, 1055 (1988).
[82] L. J. Overzet and L. Luo, Appl. Phys. Lett. **59**, 161 (1991).
[83] K. Becker (private communication, 2000).
[84] H. Deutsch, K. Becker, and T. D. Märk, Int. J. Mass Spectrom. Ion Processes **167/168**, 503 (1997).
[85] M. Probst, H. Deutsch, K. Becker, and T. D. Märk, Int. J. Mass Spectrom. Ion Processes **206**, 13 (2001).
[86] Y.-K. Kim and K. K. Irikura, *Atomic and Molecular Data and Their Applications*, edited by K. A. Berrington and K. L. Bell (American Institute of Physics, New York, 2000), p. 220.
[87] J. E. Hesser, J. Chem. Phys. **48**, 2518 (1968).
[88] F.-W. Breitbarth, Plasma Chem. Plasma Process. **12**, 261 (1992).
[89] G. R. Scheller, R. A. Gottscho, T. Intrator, and D. B. Graves, J. Appl. Phys. **64**, 4384 (1988).
[90] F.-W. Breitbarth and E. Ducke, Contrib. Plasma Phys. **30**, 691 (1990).
[91] M. L. Mandich, C. E. Gaebe, and R. A. Gottscho, J. Chem. Phys. **83**, 3349 (1985).
[92] R. A. Gottscho, Phys. Rev. A **36**, 2233 (1987).
[93] Z. Lj. Petrović, W. C. Wang, M. Suto, J. C. Han, and L. C. Lee, J. Appl. Phys. **67**, 675 (1990).
[94] C. E. Gaebe, T. R. Hayes, and R. A. Gottscho, Phys. Rev. A **35**, 2993 (1987).
[95] C. B. Fleddermann and G. A. Hebner, J. Vac. Sci. Technol. A **15**, 1955 (1997).
[96] L. G. Christophorou and J. K. Olthoff, Adv. Atom. Mol. Opt. Phys. **44**, 155 (2000).
[97] L. G. Christophorou, D. L. McCorkle, and L. G. Christophorou, *in Electron Molecule Interactions and their Applications* (Academic, New York, 1984), Vol. 2, Chap. 6.
[98] L. G. Christophorou and P. G. Datskos, Int. J. Mass Spectrom. Ion Processes **149/150**, 59 (1995).
[99] C. A. Moore, G. P. Davis, and R. A. Gottscho, Phys. Rev. Lett. **52**, 538 (1984)
[100] H. B. Milloy and R. W. Crompton, Phys. Rev. A **15**, 1847 (1977).
[101] R. J. Nygaard, J. Fletcher, S. R. Hunter, and S. R. Foltyn, Appl. Phys. Lett. **32**, 612 (1978).